Progress In Electromagnetics Research C, Vol. 93, 79–92, 2019

An Artificial Neural Network Approach to DoA Estimation and Switched Beamforming in Rectangular Array Based Smart Antennas

Robert Macharia[1, *], Phillip Kibet[1], and Peter Kihato[2]

Abstract—Switched beamforming using electronic phase shifters is commonplace. Digital switched beamformers offer a premise of better performance than electronic phase shift switched beamformers. It is also worth noting that current unknown signal Direction of Arrival (DoA) estimation methods (commonly MUltiple SIgnal Classification (MUSIC) and Estimation of Signal Parameters via Rotational Invariance Techniques (ESPRIT)) are generally computationally intensive. In this paper, signal DoA estimation and digital switched beamforming using aptly designed Artificial Neural Network (ANN) classifiers are looked into. Initially, signals detected at a rectangular receiving array are mapped onto a DoA through an ANN classifier. A second ANN classifier maps the selected DoA onto an optimal set of beamforming weights leading to an optimal switched beamforming reception pattern. The ANN classifiers' performance in DoA estimation and beamforming is tested over a variety of trials, yielding good results. The designed ANN beamformer premises to yield high-speed and accurate switched beamforming performance, most notably in large array systems. The ANN DoA estimator/beamformer can be easily adapted to nonuniform arrays wherein closed form DoA estimation/beamforming solutions are impractical. MATLAB software environment has been used as the main analysis tool.

1. INTRODUCTION

A smart antenna is basically an antenna array with a signal processing back-end aimed at altering the respective reception (or radiation) pattern to fit desired spatial signal signatures (DoA or Direction of Departure (DoD)) [1–3]. Ideally, maximal reception (or radiation) ought to be directed towards the DoA (or DoD) of the desired signal; minimal reception (or radiation) ought to be directed towards the DoA (or DoD) of interfering signals.

Figure 1 illustrates a typical 2-dimension radiation pattern in polar form. Maximal radiation is oriented towards the direction $\frac{3\pi}{2}$, minimal radiation towards the direction $\frac{\pi}{2}$.

Smart antennas broadly take the form of either adaptive or switched beam antenna array categories. An adaptive antenna array adapts the corresponding reception (or radiation) pattern ideally in real time to optimally fit prevailing spatial signal signatures (in the perspective of desired/interferer signal DoA). A switched beam antenna array selects a reception (or radiation) pattern from a variety of available (predefined) patterns to best-fit prevailing spatial signal signatures (in the perspective of desired/interferer signal DoA). This study involves the switched beam antenna array case.

The action of a switched beam antenna array is depicted in Fig. 2 (a simplistic illustration without indication of side-lobes).

A typical electronic switched-beam antenna array implementation is illustrated in Fig. 3.

Received 7 March 2019, Accepted 24 May 2019, Scheduled 8 June 2019

* Corresponding author: Robert Macharia (robertisaacm@gmail.com).

[1] Telecommunication and Information Engineering Department, Jomo Kenyatta University of Agriculture and Technology, Nairobi, Kenya. [2] Electrical and Electronic Engineering Department, Jomo Kenyatta University of Agriculture and Technology, Nairobi, Kenya.

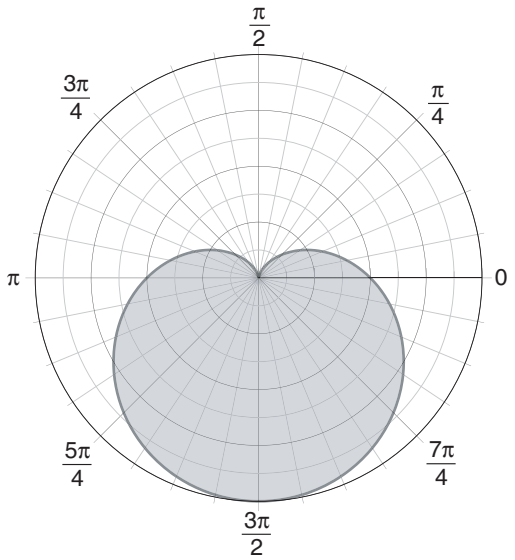

Figure 1. A typical radiation pattern plot in polar form.

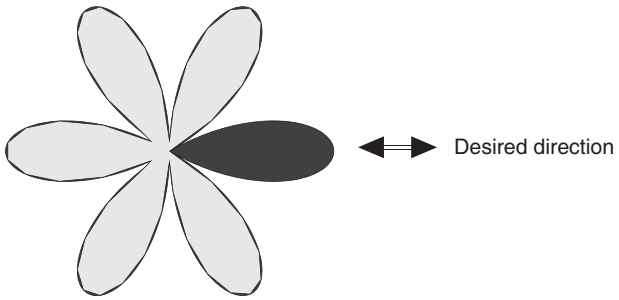

Figure 2. Switched-beam antenna array predefined radiation patterns.

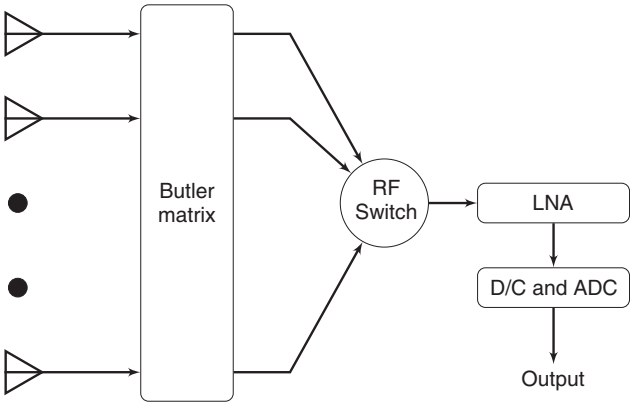

Figure 3. Switched-beam antenna array in reception mode: LNA implies low noise amplifier; DC implies down-conversion; ADC implies analogue to digital conversion.

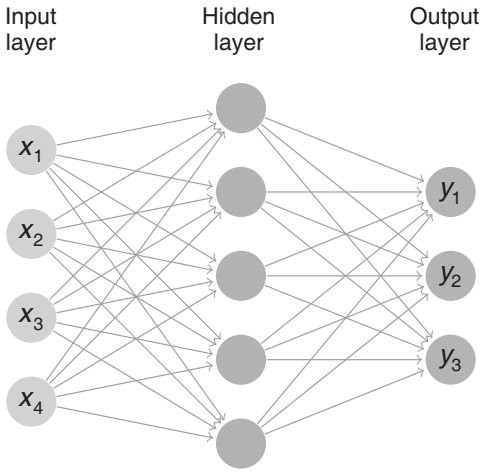

Figure 4. Structure of a typical ANN (ANN classifier).

In Fig. 3, reception patterns are synthesized using an aptly designed phase-shift network (*Butler matrix*); an action carried out at radio frequency level. A radio frequency switch selects the Butler matrix output that yields the highest Signal to Interference and Noise Ratio (SINR). A low noise amplification stage follows and consequently down-conversion to baseband/digitization to yield the desired output. A case in point utilizing a Butler matrix approach is given in [4]. In [4], a 60-GHz switched-beam patch antenna array utilizing a Butler matrix network is designed, implemented and analyzed yielding a viable and cost effective beamformer.

In [5], an electronic switched beam antenna array featuring an interleaving array architecture is presented. The corresponding analysis pinpoints viable performance.

In [6], an electronic switched beam antenna array for use in millimeter-wave communications is presented.

The work presented in [4–6] clearly cements the place of switched beam antenna array technology in modern wireless communication systems. Although switched beam antenna array technology is commonly achieved through electronic phase shifters at radio frequency level, it would be wise to research into digitally implemented switched beam antenna array technology. This is a focus of this paper: Digital switched beamforming using an ANN. Studies involving digital beam/null steering can be found in [7–9].

Procedures aimed at obtaining signal DoA in a reception array have been variably researched into, most notably MUSIC and ESPRIT algorithms. Studies involving the MUSIC signal DoA estimation method can be found in [10–12]. Studies involving the ESPRIT signal DoA estimation method can be found in [13–15]. The aforementioned signal DoA estimation procedures are typically computationally intensive. In this paper, a computationally light and real-time ANN procedure aimed at signal DoA estimation is presented.

A review of ANNs and Ant Colony Optimization (ACO) algorithm follows.

2. ARTIFICIAL NEURAL NETWORKS

2.1. Overview

In a variety of classification problems, traditional methods utilizing classical algorithms do not always give satisfactory results. Such methods are typically ineffective in situations featuring nonlinearly distributed data. The problem under consideration in this paper features nonlinearly distributed data (matching observed signals at an array to DoA and matching signal DoA to beamforming weights). ANN would be a "panacea" to the aforementioned classification problems.

2.2. Theory of ANNs

ANNs were initially developed from the perspective of the functionality of biological neural systems. ANN systems typically "learn" solutions to problems by working through presented "examples". An ANN is primarily a network of nodes by the moniker artificial neurons. An artificial neuron is basically modelled on the basis of a biological neuron. Neurons in an ANN are typically organized in layers (input, hidden and output layers) [16–18]. In Fig. 4 is an illustration of a typical ANN.

In Fig. 4, the input layer comprises 4 neurons representative of some 4 independent inputs. The hidden layer is made up of 5 neurons. The output layer comprises of 3 neurons representative of some 3 classifications. There is full connection between input-hidden layer neurons and between hidden-output layer neurons. Each and every connection between neurons bears some weight factor. The weight factors are usually modified in an ANN training process in accordance to some presented data.

Figure 5 illustrates the structure of an artificial neuron. The neuron features some 3 weighted inputs. The output observed from the neuron can be expressed as per Eq. (1), where f is the

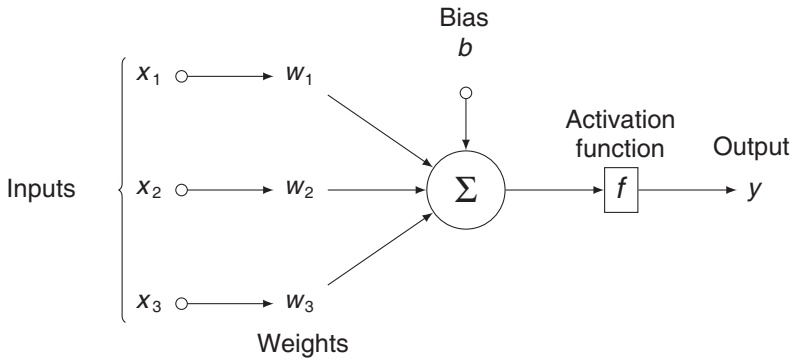

Figure 5. The operation and structure of a single neuron.

representative of the activation function.

$$y = f\left(\sum_{k=1}^{3} x_k w_k\right) \tag{1}$$

3. ANT COLONY OPTIMIZATION ALGORITHM

In this paper, the ACO algorithm has been utilized in a step geared towards creating ANN beamformer training data as well as in ANN beamformer performance validation. The ACO algorithm is based on the behavior of ants in a natural environment.

In a natural environment, ants foraging for food initially roam randomly from their colonies. Upon obtaining a food source, an ant finds its way back to its colony whilst laying down a pheromone trail. Any other ant that encounters the pheromone laden path follows it rather than taking a random path resulting in pheromone reinforcement if it successfully obtains the expected food. With time, pheromone evaporates from paths reducing their attractiveness, more so in long paths. Short paths end up being more and more attractive/pheromone laden. From an artificial optimization perspective, pheromone evaporation inherently prevents premature convergence. Reference can be made to [19–21].

The ACO algorithm mimics the aforementioned natural ant behavior. In the ACO algorithm, an ant plays the role of the chief computation agent. Associated with an ant is a solution to the optimization problem under consideration. An ant can be framed as having moved from some solution state x to some other solution state y over a single iteration. In each and every iteration, an ant k computes a set of viable solution states; A probabilistic selection of the subsequent state is made from the set. Generally, the kth ant moves from some solution state x to some subsequent solution state y with the probability defined in Eq. (2).

$$p_{xy}^{k} = \frac{(\tau_{xy}^{\alpha})(\eta_{xy}^{\beta})}{\sum_{z \in \text{allowed}_y}(\tau_{xz}^{\alpha})(\eta_{xz}^{\beta})} \tag{2}$$

In Eq. (2),

- τ_{xy} is the representative of the amount of pheromone deposited in a transition from solution state x to solution state y
- α is a control on the impact of τ_{xy}
- η_{xy} is the representative of the desirability of state transition xy (typically obtained from $1/d_{xy}$, where d is the representative of distance)
- β is a control on the impact of of η_{xy}
- τ_{xz} and η_{xz} are the representatives of the attractiveness and trail levels respectively of the other potential state transitions.

Consequently, pheromone trails are updated as per Eq. (3).

$$\tau_{xy} \leftarrow (1-\rho)\tau_{xy} + \sum_{k} \Delta\tau_{xy}^{k} \tag{3}$$

In Eq. (3),

- τ_{xy} is the representative of the amount of pheromone deposited for a transition from solution state x to solution state y
- ρ is the representative of a pheromone evaporation coefficient
- $\Delta\tau_{xy}^{k}$ is the representative of the amount of pheromone deposited by the kth ant

Figure 6 is representative of an ACO algorithm flowchart.

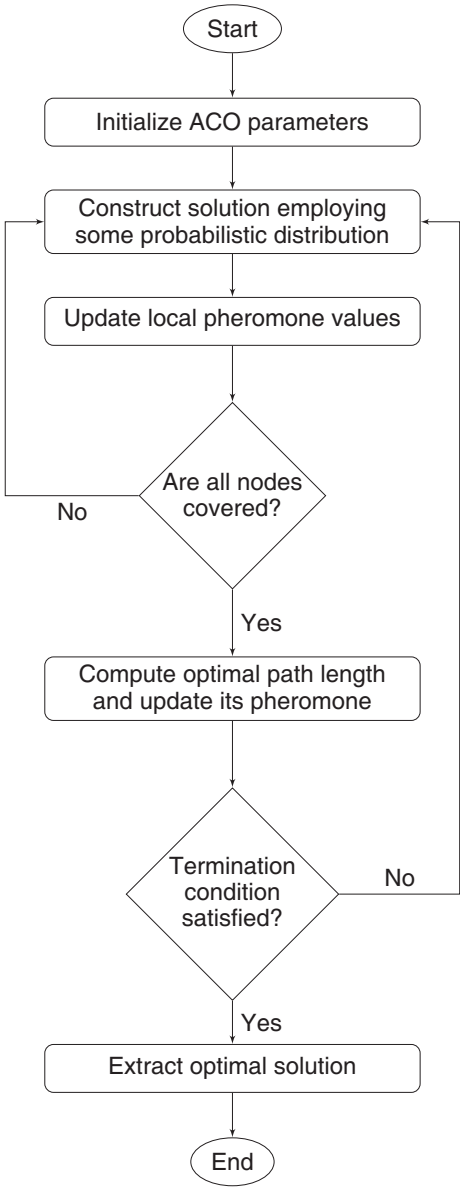

Figure 6. ACO algorithm flowchart.

4. METHODOLOGY

4.1. Beamformer Structure Design

Figure 7 illustrates the designed beamformer structure (implemented in a MATLAB software environment).

In Fig. 7:

- s denotes the desired signal.
- $(\theta,\ \phi)$ denotes the signal DoA.
- w denotes the beamformer weight.
- x denotes the signal observed at some array element.
- y denotes the beamformer output.

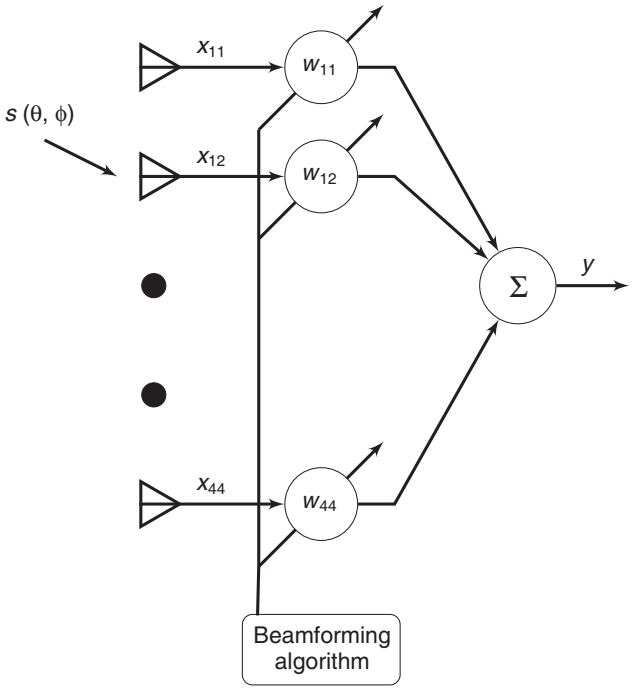

Figure 7. Designed beamformer structure.

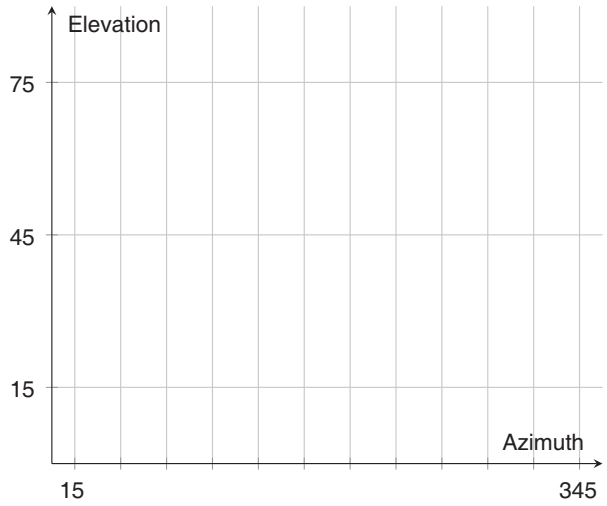

Figure 8. Adopted DoA subdivision scheme. Each grid intersection point represents a selected elevation/azimuth angle pair. Total count = 36 points.

The array is modeled as a planar 4 by 4 arrangement of isotropic receivers. The corresponding array response vector $\bar{a}(\theta,\ \phi)$ is as per Eq. (4).

$$\bar{a}(\theta,\ \phi) = [a_{11}(\theta,\ \phi) \quad a_{12}(\theta,\ \phi) \quad a_{13}(\theta,\ \phi) \quad ... \quad a_{44}(\theta,\ \phi)]^T \tag{4}$$

$a_{mn}(\theta,\ \phi)$ is as per Eq. (5).

$$a_{mn}(\theta,\ \phi) = e^{j((m-1)(kd_x \sin(\theta)\cos(\phi))+(n-1)(kd_y \sin(\theta)\sin(\phi)))} \tag{5}$$

In Eq. (5), k denotes the wave number ($\frac{2\pi}{\lambda}$), where λ implies the wavelength. The array element separation distances d_x and d_y are fixed at $\frac{\lambda}{2}$.

The signals observed at all array channels at some time instance k ($x_{11}(k)$ to $x_{44}(k)$ as per Fig. 7) can be written succinctly as per vector $\bar{x}(k)$ presented in Eq. (6).

$$\bar{x}(k) = [\bar{a}] \cdot [s(k)] \tag{6}$$

In Eq. (6):

- $\bar{a}$ denotes the array response vector corresponding to the desired signal DoA.
- $s(k)$ denotes the desired signal at instance k.

Consequently, the beamformer output can be expressed as per Eq. (7).

$$y(k) = \bar{w}^H(k) \cdot \bar{x}(k) \tag{7}$$

In Eq. (7), $\bar{w} = [w_{11} \quad w_{12} \quad .... \quad w_{44}]$ and $\bar{x}(k)$ are the beamformer weight and signal vectors, respectively.

In this paper, the desired signal has been framed as a 4-Quadrature Amplitude Modulation (QAM) signal.

4.2. DoA Estimator Design

The design process of the ANN based DoA estimator is herein described. The DoA estimator is expected to match signals observed at array terminals to appropriate DoA. This is founded on the fact that a signal emanating from a given direction yields a unique DoA based signature on some receiving array structure (Eq. (6)).

4.2.1. ANN Training Data Generation

The ANN DoA estimator training data is created from a pool of data corresponding to the signals observed at the receiving array over a variety of DoA (Eq. (6)). The selected DoA are as per Fig. 8 (given precisely in Table 1).

Table 1. Adopted DoA subdivision scheme.

El. = 15	Az.	El. = 45	Az.	El. = 75	Az.
15	15	45	15	75	15
15	45	45	45	75	45
15	75	45	75	75	75
15	105	45	105	75	105
15	135	45	135	75	135
15	165	45	165	75	165
15	195	45	195	75	195
15	225	45	225	75	225
15	255	45	255	75	255
15	285	45	285	75	285
15	315	45	315	75	315
15	345	45	345	75	345

The signal (essentially a vector of 16 elements) observed at the receiving array is complex in nature. To allow for usage of a scalar ANN, the complex data is framed from the perspective of the real and imaginary components (yielding a vector of 32 elements).

4.2.2. ANN Design

Figure 9 illustrates the designed neural network. The network features 32 input layer neurons, 100 hidden layer neurons, and 36 output layer neurons. The input layer neurons correspond to observed array signal. The output layer neurons correspond to DoA classes as per the subdivisions highlighted in Fig. 8/Table 1.

A total of 2592 data samples are utilized (using data framed as per Section 4.2.1). 90 percent of the samples (2332) are utilized in the ANN training stage, 5 percent of the samples (130) in the validation stage and 5 percent of the samples (130) in the testing stage.

The ANN is trained using the scaled conjugate gradient back-propagation method.

4.3. Beamformer Design

The design process of the ANN based beamformer is herein described. The beamformer is expected to match DoA to appropriate beamformer weights yielding optimal reception patterns.

4.3.1. ANN Training Data Generation

Initially, beamformer weights are generated on the basis of an ACO algorithm solution to a reference signal beamforming problem (8).

$$y(k) = d(k) - \bar{w}^H(k) \cdot \bar{x}(k) \tag{8}$$

where $d(k)$ is some training (reference) signal of convenient length.

The ACO algorithm is invoked to minimize Eq. (8) with beamformer weights w as variables. Optimal weights generate an optimal reception pattern. Essentially, beamformer weights corresponding to a set of pre-selected DoA are inherently obtained. The selected DoA are as per Fig. 8 (given precisely in Table 1). The DoAs are at 30 degrees intervals in both elevation and azimuth directions within the elevation range [15–75 degrees] and azimuth range [15–345 degrees].

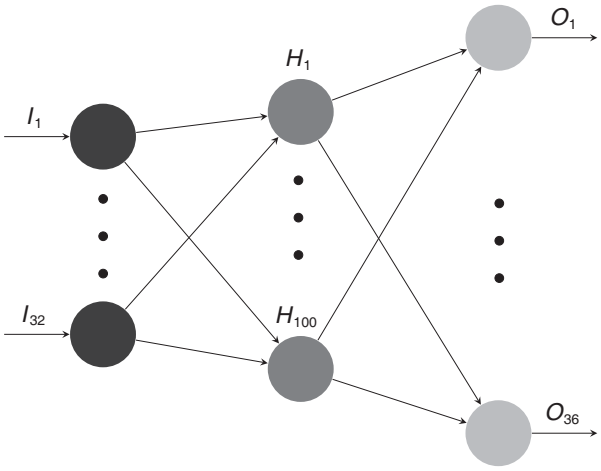

Figure 9. Designed ANN structure.

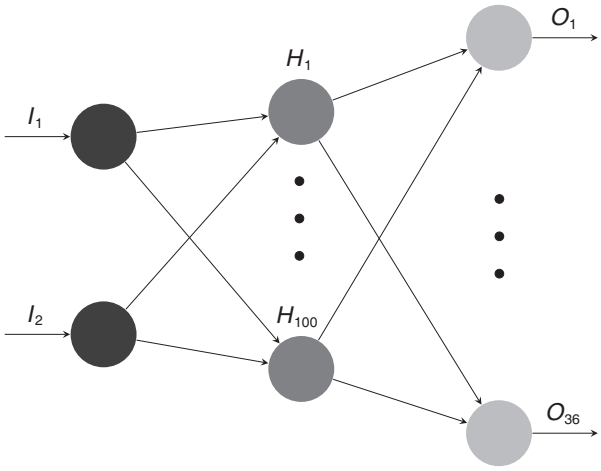

Figure 10. Designed ANN structure.

4.3.2. ANN Design

Figure 10 illustrates the designed neural network. The network features 2 input layer neurons, 100 hidden layer neurons, and 36 output layer neurons. The input layer neurons correspond to elevation and azimuth angle pairs. The output layer neurons correspond to beamforming weights classes as per the subdivisions highlighted in Fig. 8/Table 1.

A total of 2592 data samples are utilized (using data framed as per Section 4.3.1). 90 percent of the samples (2332) are utilized in the ANN training stage, 5 percent of the samples (130) in the validation stage and 5 percent of the samples (130) in the testing stage.

The ANN is trained using the scaled conjugate gradient back-propagation method.

5. RESULTS

The performance of the designed ANN DoA estimator and ANN beamformer is tested in a variety of trials. The results obtained are presented herein.

5.1. DoA Estimation

The desired signal is assigned a variety of randomly selected DoA (as per column *Exact DoA* in Table 2). The designed ANN DoA estimator yields the results depicted in column *ANN obtained DoA* in Table 2. It is worth noting that the ANN DoA estimator yields accurate results in real-time. *Exact DoA* implies the actual DoA associated with the desired signal. The *ANN obtained DoA* is an approximate DoA value (ideally as close as possible to the *Exact DoA*).

Table 2. Select DoA estimation results.

	Exact DoA		ANN obtained DoA	
	Azimuth	Elevation	Azimuth	Elevation
Trial 1	40	15	45	15
Trial 2	180	10	165	15
Trial 3	300	15	285	15
Trial 4	50	45	45	45
Trial 5	190	50	195	45
Trial 6	320	55	315	45
Trial 7	43	70	45	75
Trial 8	187	75	195	75
Trial 9	290	80	285	75
Trial 10	180	45	195	45

5.2. Switched Beamforming

The results obtained upon utilizing the designed ANN in switched beamforming are herein presented.

In the first trial, the desired signal features the DoA (40, 15). An ANN DoA estimator yields a DoA (45, 15). The subsequent ANN beamforming process yields the results depicted in Fig. 11. The resultant relative reception strength in the DoA (40, 15) is −2.31 dB. In comparison to an ACO based reference signal beamformer (as per Eq. (8)) relative reception strength in the DoA (40, 15) (−0.25 dB), the −2.31 dB figure is 2.06 dB off. The small loss in reception strength is allowable in low noise channels if at all gains are to be made from the high speed action of the ANN beamformer.

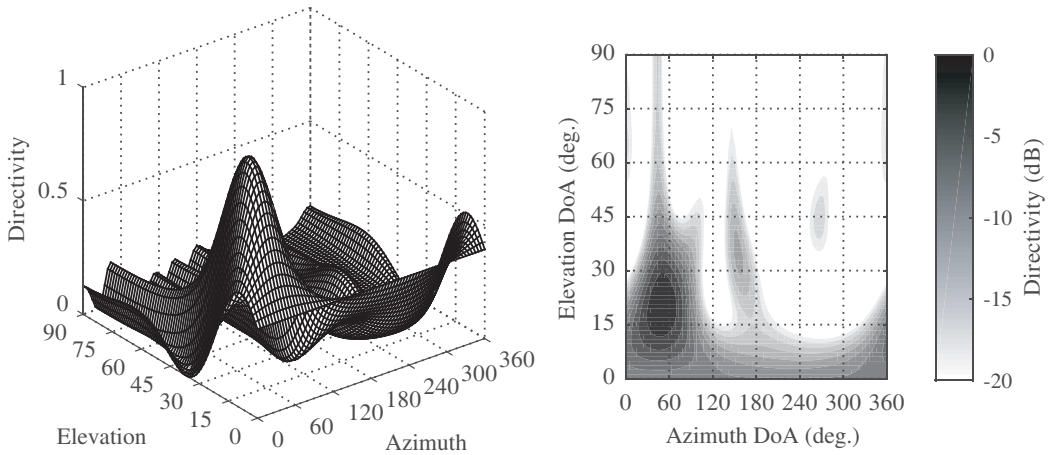

Figure 11. Reception pattern in the form of contour and mesh plots. The main beam is oriented ideally towards the DoA (45, 15) degrees.

In the second trial, the desired signal features the DoA (180, 10). An ANN DoA estimator yields a DoA (165, 15). The subsequent ANN beamforming process yields the results depicted in Fig. 12. The resultant relative reception strength in the DoA (180, 10) is −4.35 dB. In comparison to an ACO based reference signal beamformer (as per Eq. (8)) relative reception strength in the DoA (180, 10) (−0.93 dB), the −4.35 dB figure is 3.42 dB off. The small loss in reception strength is allowable in low noise channels if at all gains are to be made from the high speed action of the ANN beamformer.

In the third trial, the desired signal features the DoA (300, 15). An ANN DoA estimator yields

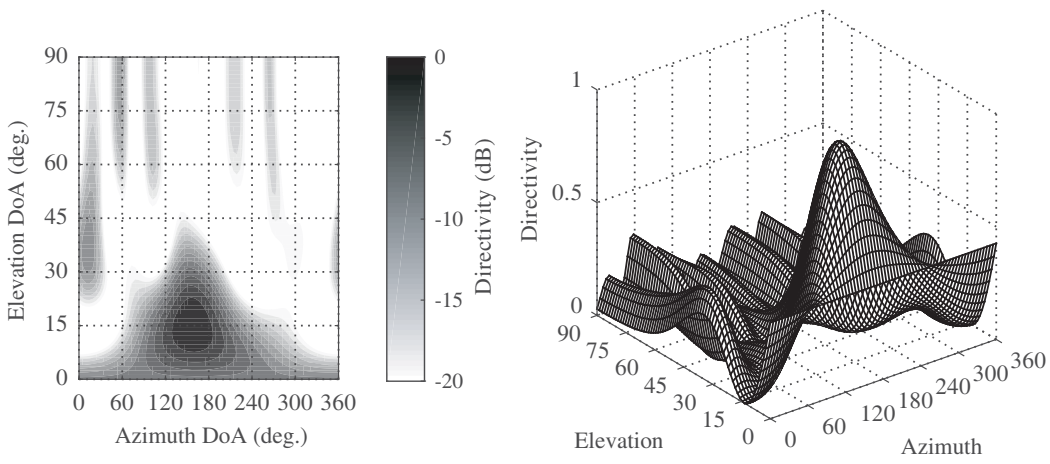

Figure 12. Reception pattern in the form of contour and mesh plots. The main beam is oriented ideally towards the DoA (165, 15) degrees.

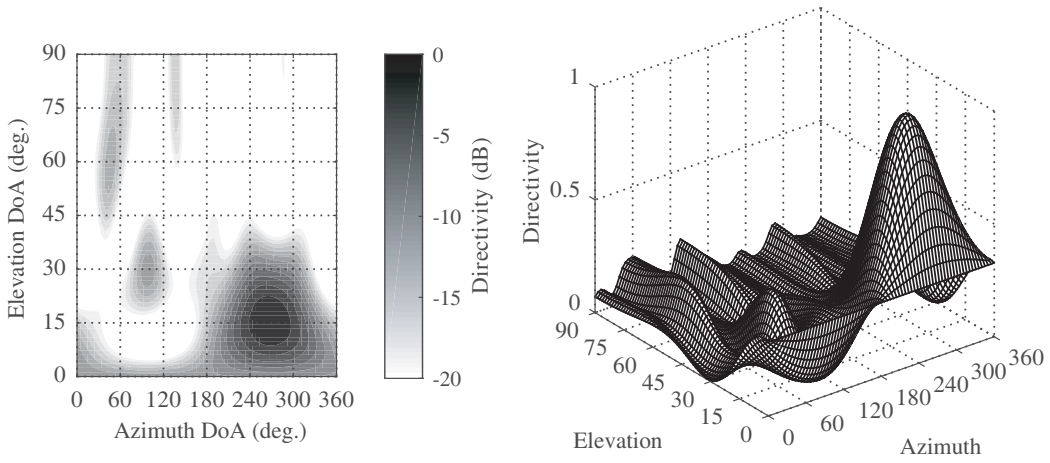

Figure 13. Reception pattern in the form of contour and mesh plots. The main beam is oriented ideally towards the DoA (285, 15) degrees.

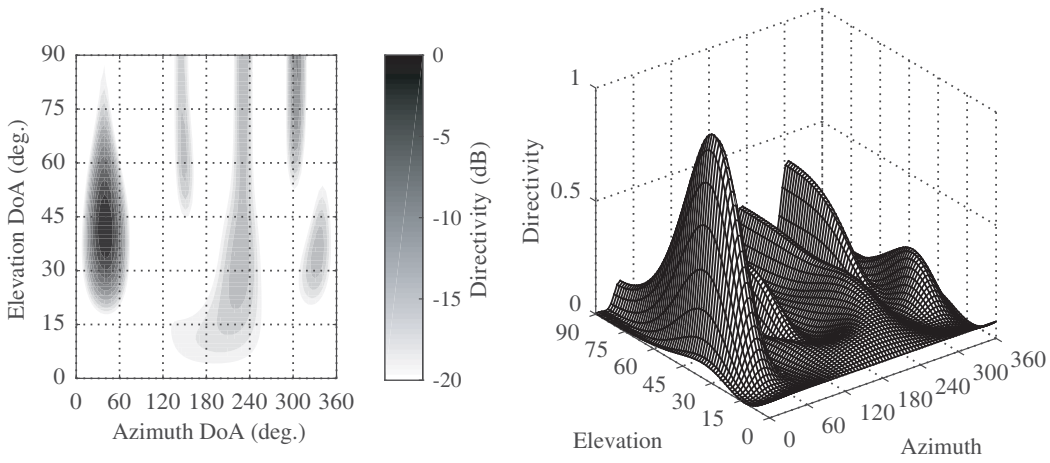

Figure 14. Reception pattern in the form of contour and mesh plots. The main beam is oriented ideally towards the DoA (45, 45) degrees.

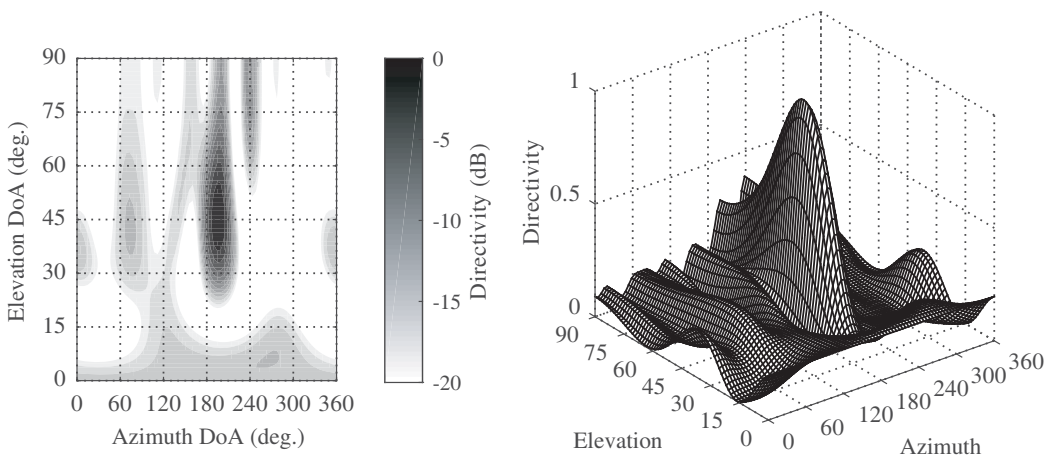

Figure 15. Reception pattern in the form of contour and mesh plots. The main beam is oriented ideally towards the DoA (195, 45) degrees.

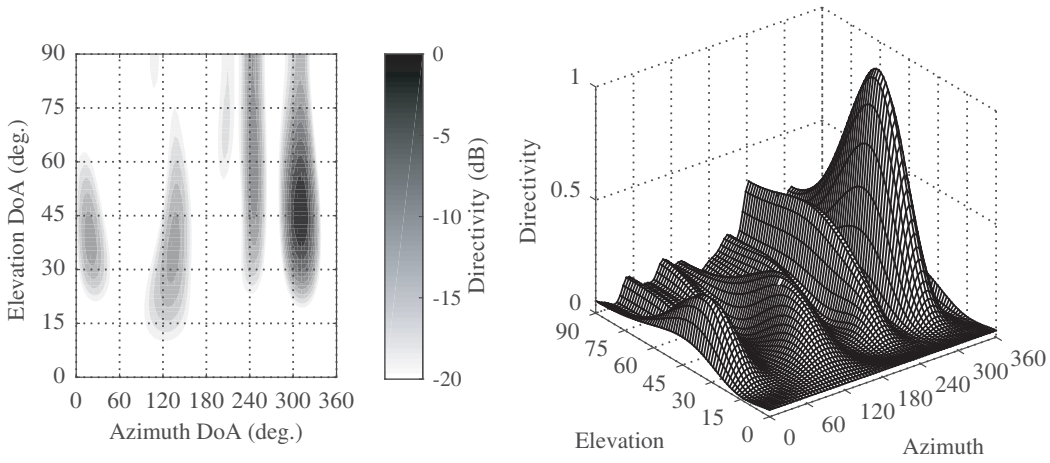

Figure 16. Reception pattern in the form of contour and mesh plots. The main beam is oriented ideally towards the DoA (315, 45) degrees.

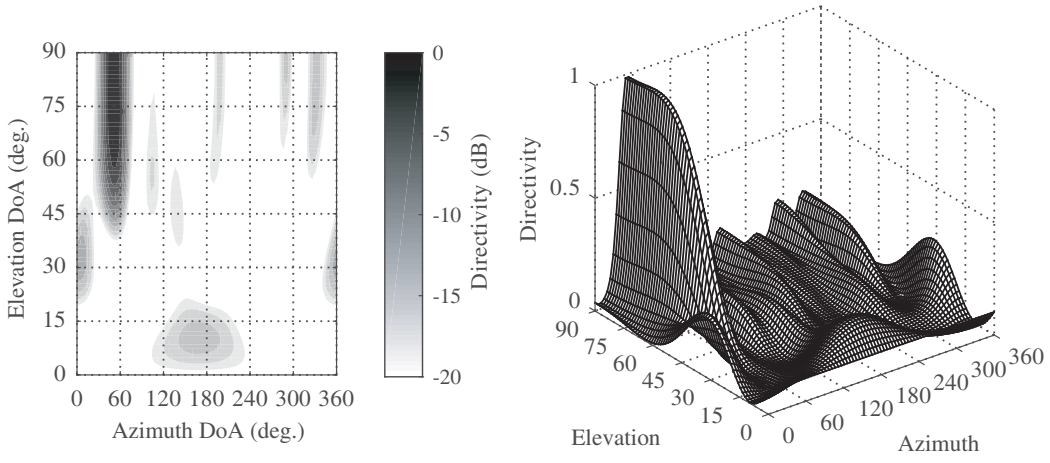

Figure 17. Reception pattern in the form of contour and mesh plots. The main beam is oriented ideally towards the DoA (45, 75) degrees.

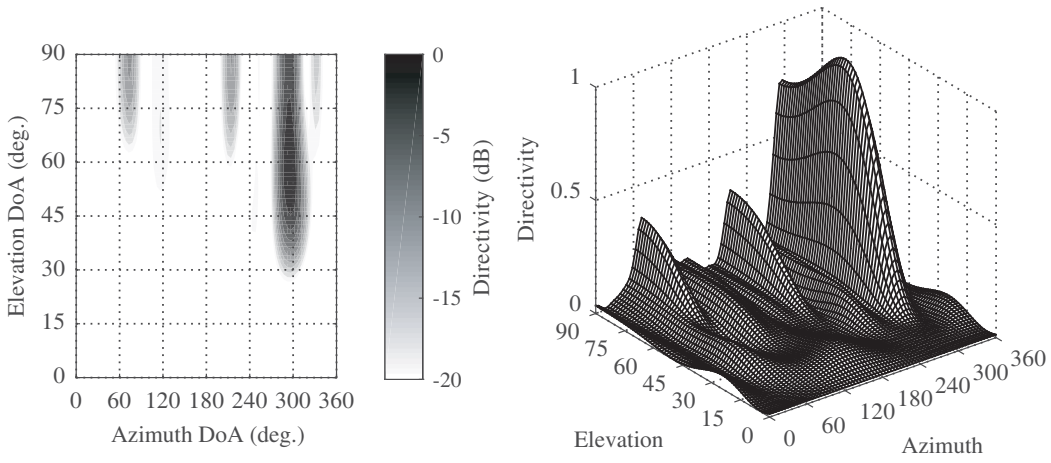

Figure 18. Reception pattern in the form of contour and mesh plots. The main beam is oriented ideally towards the DoA (295, 75) degrees.

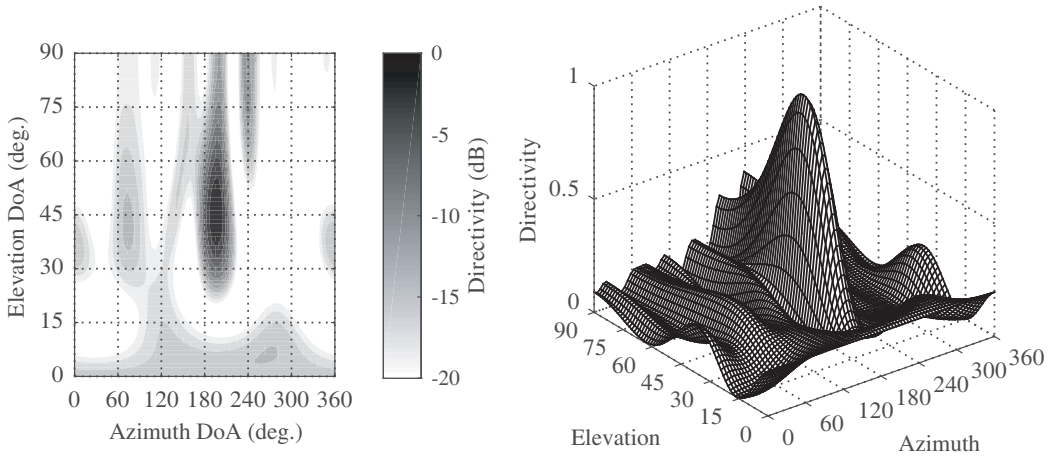

Figure 19. Reception pattern in the form of contour and mesh plots. The main beam is oriented ideally towards the DoA (180, 45) degrees.

Table 3. Relative reception strength data (in dB) over a variety of DoAs.

	Exact DoA		ANN DoA		Reception strength		
	Az.	El.	Az.	El.	ACO Ref. Sig.	ANN	Deviation
Trial 1	40	15	45	15	−0.25	−2.31	2.06
Trial 2	180	10	165	15	−0.93	−4.35	3.42
Trial 3	300	15	285	15	−0.72	−4.16	3.44
Trial 4	50	45	45	45	−1.57	−4.22	2.65
Trial 5	190	50	195	45	−1.72	−3.79	2.07
Trial 6	320	55	315	45	−0.54	−4.51	3.97
Trial 7	43	70	45	75	−1.09	−4.64	3.55
Trial 8	187	75	195	75	−1.16	−4.2	3.04
Trial 9	290	80	285	75	−2.33	−4.2	1.87
Trial 10	180	45	195	45	−1.64	−4.23	2.59

a DoA (285, 15). The subsequent ANN beamforming process yields the results depicted in Fig. 13. The resultant relative reception strength in the DoA (300, 15) is −4.16 dB. In comparison to an ACO based reference signal beamformer (as per Eq. (8)) relative reception strength in the DoA (300, 15) (−0.72 dB), the −4.16 dB figure is 3.44 dB off. The small loss in reception strength is allowable in low noise channels if at all gains are to be made from the high speed action of the ANN beamformer.

Results corresponding to other trials are captured in Figs. 14 to 19 and in Table 3.

In summary, relative reception strength data (in dB) is given in Table 3. ANN DoA estimation/beamforming is compared to an ACO algorithm aided reference signal beamforming procedure. It is worth noting that ANN DoA estimation and the subsequent ANN beamforming results in slight reception strength variation (negatively) in comparison to the ACO algorithm aided reference signal beamforming procedure. This can be attributed to the inherent ANN DoA estimation process approximations (*for instance the DoA (40, 15) being classified as (45, 15) in Trial 1 as per Table 3.*).

6. CONCLUSION

In this paper, ANN based DoA estimation and beamforming is proposed. The performance of the designed ANN DoA estimator and beamformer is tested in a variety of trials involving a rectangular array, yielding appreciably good results. The ANN solutions offer a high speed and appreciably accurate solution to switched beamforming.

The proposed solution inherently takes care of DoA estimation and beamforming on the basis of irregularly shaped nonuniform arrays wherein closed form solutions to beam steering are impossible. Usage of the proposed ANN based DoA estimator/beamformer would ideally be limited to propagation environments bearing minimal multi-path propagation changes. Retraining would be necessary in environments bearing an appreciable degree of multi-path propagation changes.

REFERENCES

1. Gross, F. B., *Smart Antennas for Wireless Communications*, 2nd Edition, McGraw-Hill, New York, 2015.
2. Chand-Godara, L., *Smart Antennas*, 1st Edition, CRC Press, Boca Raton, Florida, 2002.
3. Allen, B. and M. Ghavami, *Adaptive Array Systems Fundamentals and Applications*, 1st Edition, John Wiley and Sons, Hoboken, New Jersey, 2005.
4. Tseng, C. H., C. J. Chen, and T. H. Chu, "A low-cost 60-GHz switched-beam patch antenna array with butler matrix network," *IEEE Antennas and Wireless Propagation Letters*, Vol. 7, 432–435, 2008.
5. Wang, H., Z. Zhang, Y. Li, and M. F. Iskander, "A switched beam antenna with shaped radiation pattern and interleaving array architecture," *IEEE Transactions on Antennas and Propagation*, Vol. 63, No. 7, 2914–2921, Jul. 2015.
6. Semkin, V., F. Ferrero, A. Bisognin, J. Ala-Laurinaho, C. Luxey, F. Devillers, and A. V. Räisänen, "Beam switching conformal antenna array for mm-wave communications," *IEEE Antennas and Wireless Propagation Letters*, Vol. 15, 28–31, 2016.
7. Magalhaes, M. P., A. M. Engroff, L. S. Pereira, M. V. T. Heckler, and A. G. Girardi, "Synthesis of the radiation pattern of retrodirective antenna arrays using the particle swarm optimization algorithm," *2015 SBMO IEEE MTT-S International Microwave and Optoelectronics Conference (IMOC)*, 1–5, Nov. 2015.
8. Saxena, P. and A. Kothari, "Ant lion optimization algorithm to control side lobe level and null depths in linear antenna arrays," *AEU — International Journal of Electronics and Communications*, Vol. 70, No. 9, 1339–1349, 2016.
9. Rahman, S. U., Q. Cao, M. M. Ahmed, and H. Khalil, "Analysis of linear antenna array for minimum side lobe level, half power beamwidth, and nulls control using PSO," *Journal of Microwaves, Optoelectronics and Electromagnetic Applications*, Vol. 16, 577–591, Apr. 2017.

10. Gao, Y., X. Jia, J. Xu, T. Long, and X.-G. Xia, "A novel DOA estimation method for closely spaced multiple sources with large power differences," *2015 IEEE Radar Conference (RadarCon)*, 1276–1279, May 2015.
11. Bartoli, G., R. Fantacci, D. Marabissi, and M. Pucci, "LTE-A femto-cell interference mitigation with music DOA estimation and null steering in an actual indoor environment," *2013 IEEE International Conference on Communications (ICC)*, 2707–2711, Jun. 2013.
12. Yan, F., M. Jin, and X. Qiao, "Low-complexity doa estimation based on compressed music and its performance analysis," *IEEE Transactions on Signal Processing*, Vol. 61, No. 8, 1915–1930, Apr. 2013.
13. Cui, K., W. Wu, J. Huang, X. Chen, and N.-C. Yuan, "2-D DOA estimation of LFM signals for uca based on time-frequency multiple invariance esprit," *Progress In Electromagnetics Research M*, Vol. 53, 153–165, 2017.
14. Lavate, T., V. Kokate, and A. M. Sapkal, "Performance analysis of music and esprit DOA estimation algorithms for adaptive array smart antenna in mobile communication," *Second International Conference on Computer and Network Technology*, 308–312, 2010.
15. Wu, Y., A. Leshem, J. R. Jensen, and G. Liao, "Joint pitch and DOA estimation using the esprit method," *IEEE/ACM Transactions on Audio, Speech, and Language Processing*, Vol. 23, No. 1, 32–45, Jan. 2015.
16. Hassoun, M., *Fundamentals of Artificial Neural Networks*, 1st Edition, MIT Press, Cambridge, Massachusetts, 2003.
17. Anthony, M., *Neural Network Learning: Theoretical Foundations*, 1st Edition, Cambridge University Press, Cambridge, United Kingdom, 2009.
18. Haykin, S., *Neural Networks and Learning Machines*, 3rd Edition, Pearson, London, United Kingdom, 2008.
19. Dorigo, M. and M. Birattari, *Ant Colony Optimization*, 36–39, Springer US, Boston, MA, 2010.
20. Zhang, X., S. Wang, L. Yi, H. Xue, S. Yang, and X. Xiong, "An integrated ant colony optimization algorithm to solve job allocating and tool scheduling problem," *Proceedings of the Institution of Mechanical Engineers, Part B: Journal of Engineering Manufacture*, Vol. 232, No. 1, 172–182, 2018.
21. Sama, M., A. D'Ariano, D. Pacciarelli, P. Pellegrini, and J. Rodriguez, "Ant colony optimization for train routing selection: Operational vs tactical application," *2017 5th IEEE International Conference on Models and Technologies for Intelligent Transportation Systems (MT-ITS)*, 297–302, Jun. 2017.